MetaGXplore: Integrating Multi-Omics Data with Graph Convolutional Networks for Pan-cancer Patient Metastasis Identification

Tao Jiang[a,1], Haiyang Jiang[b,1], Xinyi Ma[c], Minghao Xu[a], Wentao Zhang[a,*]

[a] *Center for Machine Learning Research, Peking University, China*
[b] *University of Queensland, Australia*
[c] *Institute of Entomology, Guizhou University, China*

Abstract

Objective: Tumor metastasis, the spread of cancer cells from the primary tumor to distant anatomical sites, poses a significant challenge in clinical prognosis, impairing treatment efficacy and reducing patient survival time. Current methods for predicting and diagnosing tumor metastasis rely heavily on extensive examinations and subjective clinical judgments, introducing considerable uncertainty and inefficiency. Accurate prediction of tumor metastasis likelihood is crucial for guiding effective clinical interventions and extending patient survival. Additionally, identifying key genes that influence metastasis probability could provide valuable data for detecting tumor-specific biomarkers indicative of metastasis likelihood.

Methods: Multi-omics datasets, which encompass diverse genomic information, offer a comprehensive understanding of cancer biology. Leveraging deep learning algorithms enhances the accuracy and predictive power in forecasting cancer metastasis, given their superior performance in complex prediction tasks. We developed a deep learning-based framework, MetaGXplore, which represents the first attempt to predict metastasis probability using pan-cancer multi-omic datasets and to explain the pivotal genes involved in the process.

Conclusions: We trained the classification model using a K-fold cross-validation procedure and interpreted the predicted results with GNNExplainer. The effectiveness of MetaGXplore was demonstrated by evaluating the model, graph structure contribution, and multi-omics data. Finally, enrichment analysis of differentially expressed genes and pathways was conducted to explore the biological functions of major differential genes and the relationships between key pathways.

Key words: Tumor metastasis, pan-cancer, multi-omics, deep learning, graph convolutional network.

* Corresponding author at: Center for Machine Learning Research, Peking University, China
E-mail addresses: wentao.zhang@pku.edu.cn (Wentao Zhang)
[1] Equal contribution

Introduction

Cancer metastasis, a critical hallmark of malignancy associated with tumor progression and poor patient prognosis, involves the dissemination of cancer cells from the primary tumor to distant organs. Metastasis presents a formidable challenge in cancer management, often signifying advanced tumor progression and adversely affecting patient survival outcomes. Conventional methods for identifying tumor metastasis primarily rely on histopathological examinations, imaging techniques, and clinical discoveries. While these methods provide relatively accurate assessments of overt metastasis, they depend heavily on the expertise of healthcare professionals and may lack sensitivity in detecting micrometastasis or accurately predicting metastatic risk [1-7]. Consequently, there is an urgent need for innovative tools that offer convenient and rapid assessment of tumor metastatic risk to aid clinical management [8-10].

In recent years, leveraging artificial intelligence (AI), particularly deep learning methods, has emerged as a transformative approach in disease research and clinical practice. AI-based predictive models utilizing multi-omics data have shown significant potential across various applications. The advancement of high-throughput sequencing technology and the advent of multi-omics sequencing have exponentially increased the molecular characteristics that can be used as features and insights into pathophysiology [11-14]. However, the inherent heterogeneity of cancer results in diverse molecular characteristics among patients. This patient-specific molecular signature can be conceptualized as a unique subnetwork within the broader molecular network, representing individual genetic features [3]. Integrating and transforming these patient genetic features into patient-specific networks allows for deeper insights, improving the detection of tumor metastasis risk through AI-driven analysis and enhancing prognostic treatment strategies. Current approaches for predicting cancer metastasis using machine learning face significant challenges, such as the high dimensionality of data points representing individual patient features from multi-omics datasets [15]. This "curse of dimensionality" leads to instability in the feature selection process across different datasets. Recently, graph convolutional neural networks (GCNs) have been widely adopted for processing graph signal classification tasks, effectively addressing the "curse of dimensionality" [16, 17]. Furthermore, interpreting deep learning model predictions within a genetic context is essential, especially given regulatory requirements like the European Union's General Data Protection Regulation (GDPR), which imposes restrictions on automated decisions generated by algorithms [18]. The interpretability of deep neural networks is thus a critical factor in enhancing confidence in AI model predictions and understanding the mechanisms underlying tumor metastasis.

In this study, we introduce MetaGXplore, a novel deep learning model that integrates Graph Convolutional Networks (GCNs) with multi-omics pan-cancer data to predict metastasis. Our model was trained and tested on a dataset comprising 754 samples from 11 cancer types, each with balanced evidence of metastasis and non-metastasis. The results demonstrate MetaGXplore's superior performance compared to other deep learning

methods such as Multi-Layer Perceptron (MLP) and transformers. Additionally, to enhance MetaGXplore's interpretability, we employed Graph Mask and Feature Mask methods from GNNExplainer. These techniques elucidated the model's inner workings and identified key genes associated with metastasis. Subsequently, pathway enrichment analysis provided insights into the functions of these genes and explored their interactions within Protein-Protein Interaction (PPI) networks, supplemented by literature reviews to comprehensively interpret their roles. Overall, our study advances the application of AI and multi-omics data in clinical treatment strategy selection and provides a valuable gene set for future research on tumor metastasis.

Materials and Methods

Data collection and preprocessing

We collected primary samples from 33 different cancers from The Cancer Genome Atlas (TCGA) projects, each with and without distant metastasis. The dataset includes mRNA, methylation, and mutation data. Specifically, we focused on 11 cancer types where all three types of omics data are available simultaneously. Among the datasets, 754 samples were used for modeling, comprising 377 samples diagnosed with metastatic cancer and an equal number of 377 samples diagnosed with primary tumors without evidence of metastasis. The categorization of distant metastasis status follows the American Joint Committee on Cancer (AJCC) guidelines, with M0 assigned to samples without evidence of distant metastasis and M1 to those that show such evidence (4). Equal counts are evident for both metastatic and in situ cancers, as depicted in the table (Table 1).

Table 1. Distribution of cancer tumor types and sample counts in metastatic.

Cancer types	**Abbreviation**	**Sample counts**	**Cancer types**	**Abbreviation**	**Sample counts**
Bladder Urothelial Carcinoma	BLCA	2	Pancreatic adenocarcinoma	PAAD	3
Breast invasive carcinoma	BRCA	9	Pheochromocytoma and Paraganglioma	PCPG	3
Cervical squamous cell carcinoma endocervical adenocarcinoma	CESC	2	Prostate adenocarcinoma	PRAD	2
Colon adenocarcinoma	COAD	2	Skin Cutaneous Melanoma	SKCM	343
Esophageal carcinoma	ESCA	2	Thyroid carcinoma	THCA	6
Head and Neck squamous cell carcinoma	HNSC	3			

The multi-omic datasets were acquired using the TCGA-biolinks R package, enabling access to the Genomic Data Commons (GDC) Data Portal (2; 8). Utilizing both the TCGA-biolinks and TCGA-assembler packages, we conducted preprocessing on the harmonized TCGA dataset. Initially, we mapped CpG islands within 1500 bp upstream of gene transcription start sites (TSS) and computed average methylation values. To

address missing values, we implemented three preprocessing steps based on a reported approach (1). First, we excluded genes (e.g., mRNA/DNA methylation) with zero values in more than 25% of patients. Next, we filtered out samples with less than 75% of the remaining features. For mutation data, we excluded features with zero occurrences across all samples and filtered out features with zeros in more than 40% of patients. Finally, we employed the R impute function (7) to impute missing expression data using nearest neighbor averaging to fill the remaining gaps. Each test set underwent independent preprocessing. After preprocessing, there were 377 metastatic samples encompassing all three data types. For interpretability purposes, we retained genes featuring all three omics data types and randomly selected an equivalent number of non-metastatic samples for statistical analysis.

To transform omics data into a graph format, each patient can be represented as a graph: G={G_1,G_2,…,G_N }, where N is the number of patients. For an arbitrary graph $\mathcal{G}_i = (\mathcal{V}_i, \xi_i, X_i, Y_i)$, $\mathcal{V}_i$ and ξ_i denote the nodes and edges, which represent genes and protein-protein interactions, respectively. $X_i \in \mathbb{R}^{n_i \times f}$ is the node feature matrix, where |V_i |=n_i is the number of genes, and f is the number of omics features. Y_i is the label of the ith graph, with Y_i = 1 if the ith patient has metastasized and Y_i=0 otherwise. Constructed by ξ_i, $A_i \in \mathbb{R}^{n_i \times n_i}$ is the adjacency matrix describing the graph's edge connection information.

Node embedding extractor

Multi-head attention mechanism in Transformer

Owing to its outstanding expressive ability, the multi-head attention mechanism is the most crucial component in transformers for extracting embeddings from text or image data. Recently, some research has applied this model to graph data problems. The vanilla transformer [19] calculates pairs of attention weights among all data entities and updates the embeddings according to the weights from all other data entities. However, this type of transformer model does not account for graph structure information. To capture topological information, the graph transformer [20] calculates attention only between nodes and their neighbors:

$$w_{ij}^{k,l} = softmax_j\left(\frac{Q^{k,l}x_i^l \cdot K^{k,l}x_j^l}{\sqrt{d_k}}\right) \tag{1}$$

$$\hat{x}_i^{l+1} = O^l \parallel_{k=1}^{H}\left(\sum_{j\in\mathcal{N}_i} w_{ij}^{k,l}V^{k,l}x_j^l\right) \tag{2}$$

In equation (1), in lth layer, x_i^l and x_j^l represent features of current node i and neighbor nodes of i. The kth weight $w_{ij}^{k,l}$ determines the importance of node i and neighbor j and is obtained by node vector dot product after the linear transformed of learnable parameters (Q, K), and this weight is normalized by dimension of node features. In equation (2), H means parallel attention mechanisms with different parameter initialization to improve the stability and generalization ability when train the model. Neighbor features that are linear

transformed by trainable weight $V^{k,l}$ are weighted summed and H heads are concatenated. Dimension of this result is H times than the input feature and the learnable matrix O^l are used to map this high dimension feature matrix to the same dimension as the input feature. As for vanilla transformer, node j means nodes other than node i.

Graph convolution network

GCN [21] is a graph model to extract embedding from graph data based on spectral clustering. This model needs two inputs: adjacency matrix $A \in \mathbb{R}^{n\times n}$ and multi-omics feature matrix $X \in \mathbb{R}^{n\times d}$. GCN can be built by stacking many layers, lth layer is defined as:

$$H^{(l+1)} = \sigma\left(\widetilde{D}^{-\frac{1}{2}}\tilde{A}\widetilde{D}^{-\frac{1}{2}}H^{(l)}W^{(l)}\right) \tag{3}$$

Here, $\widetilde{D}^{-\frac{1}{2}}\tilde{A}\widetilde{D}^{-\frac{1}{2}}$ denotes the normalized graph Laplacian, $\tilde{A} = A + I$ denotes adjacency matrix with added self-connections, $\widetilde{D}$ is degree matrix of $\tilde{A}$, $W^{(l)}$ is trainable weight matrix. σ denotes the nonlinear activation function, generally the ReLU activation function, and $H^{(l)}$ is the
input of each layer, and notably, $H^{(0)} = X$.

Patient M0/M classification prediction

We implemented the transformer using the Python PyTorch library (https://github.com/pytorch/pytorch) and the graph transformer and GCN using the Python PyTorch-Geometric library (https://github.com/pyg-team/pytorch_geometric). The model input includes a feature matrix and an edge index matrix, which represents the graph structure. In the classification model, we stack two node embedding extraction layers, such as GCN, fully connected layers, transformer, and graph transformer layers, each followed by a ReLU activation function. After the embedding layers, to obtain a vector containing information about the entire graph, we use a readout layer [22, 23] to aggregate node embeddings:

$$readout = \frac{1}{n}\sum_{p}^{n} X(p,:) \parallel \max_{q=1} X(:,q) \qquad \in \mathbb{R}^{1\times(2\times d)} \tag{4}$$

Finally, we use a Multilayer Perceptron (MLP) network with three fully connected layers for classification. To ensure sufficient training and prevent overfitting, we apply dropout with a rate of 0.5 in the MLP and use early stopping with a patience of 50 epochs. This means that if the validation loss does not decrease for 50 epochs, training will be halted. Other hyperparameters include a learning rate of 0.005, a weight decay of 0.0001, and a batch size of 8 graphs. The Adam algorithm, with its default parameters, is used as the optimizer, and cross-entropy loss is employed to compute the difference between the real and predicted labels.

Metastasis probability prediction explainer

GNNExplainer [24] generates interpretations for arbitrary neural networks and various mining tasks from the perspective of network structure and node attributes. It aims to identify the subgraph structures most relevant to prediction results, facilitating the interpretation of these results. Specifically, the Graph Mask and Feature Mask are used to screen structures and features, respectively. These two masks are treated as trainable matrices, randomly initialized, and combined with the original graph through element-wise multiplication. This task is then framed as an optimization problem to maximize the mutual information between the original graph's prediction and the interpretation graph.

Assuming that the selected structures and features that are most relevant to the model prediction results Y are G_s and X_s respectively, then their importance can be measured by the mutual information MI:

$$\max_{G_s} MI\big(Y, (G_s, X_s)\big) = H(Y) - H(Y|G = G_s, X = X_s) \tag{5}$$

The entropy $H(Y)$ is constant because the GCN is already trained, so maximum mutual information between prediction Y and explanation (G_s, X_s) is equal to minimum conditional entropy $H(Y|G = G_s, X = X_s)$, which can be expressed as:

$$\min_{G_s} H(Y|G = G_s, X = X_s) = -\mathbb{E}_{Y|G_s,X_s}[\log P_\Phi(Y|G = G_s, X = X_s)] \tag{6}$$

If we treat $G_s \sim \mathcal{G}$ as a random graph variable, the objective in Eq. (6) becomes:

$$\min_{\mathcal{G}} \mathbb{E}_{G_s \sim \mathcal{G}} H(Y|G = G_s, X = X_s) \tag{7}$$

This can be given by Jensen's inequality with convexity assumption, as the following upper bound:

$$\min_{\mathcal{G}} H\big(Y|G = \mathbb{E}_{\mathcal{G}}[G_s], X = X_s\big) \tag{8}$$

The conditional entropy in Equation (6) can be optimized by replacing the $\mathbb{E}_{\mathcal{G}}[G_s]$ to be optimized by a masking of the computation graph of adjacency matrix $A_c \odot \sigma(M)$, $M \in \mathbb{R}^{n\times n}$ and $F \in \mathbb{R}^{n\times 1}$ are learnable mask, $\odot$ is element wise product, and σ denotes the sigmoid that maps the mask to $[0,1]$.

In some applications, users care more about how to use trained model predict wanted labels, we can modify the conditional entropy objective in Equation (8) with a cross entropy objective between the label class and the model prediction:

$$\min_{M,F} -\sum_{c=1}^{C} \mathbf{1}[y = c] \log P_\Phi\big(Y = y|G = A_c \odot \sigma(M), X = X_c \odot \sigma(F)\big) \tag{9}$$

GNNExplainer is initialized with a trained graph model and individual graph data. For each graph, GNNExplainer is trained for 200 epochs to generate its unique feature mask and graph mask. To obtain a general explanation for the entire dataset, we determine the importance score of individual nodes by summing the scores of all input edges of a node and averaging by node degree. The node importance scores are calculated separately for the metastatic and non-metastatic classes.

Data partitioning and robustness assessment

When training the classification models, we used a stratified K-fold cross-validation procedure to divide the dataset. The dataset was randomly split into five folds, each containing an equal number of positive and negative samples. One fold was used as the testing dataset, and the remaining four folds were used as the training dataset, with half of the testing dataset reserved for validation. This resulted in 80% of the data being used for training and 10% each for validation and testing. For each split, we conducted five independent repeated experiments, and the evaluation indicators were averaged from the performances of a total of 25 models.

Before training the explainer model, we retrained the GCN model with the newly split dataset. The dataset was randomly divided into three parts: 80% for training, 10% for validation, and 10% for testing. We used the same training strategy and hyperparameters as those used in the classification model experiments. The newly trained GCN model and the entire dataset were then input into the GNNExplainer model to generate the feature mask and graph mask.

Results

A precisely metastasis probability prediction GCN tool

In classification tasks, prediction results can be categorized into four classes: true positive (TP), false positive (FP), false negative (FN), and true negative (TN). Accuracy denotes the percentage of testing samples correctly classified by the classifier and is defined as:

$$accury = \frac{TP + TN}{TP + FP + TN + FN}$$

The F1 score measures the accuracy of binary classification models, considering both precision and recall. The F1 score is the harmonic mean of precision and recall, with a maximum value of 1 and a minimum value of 0. It is defined as:

$$F1\ score = 2 \times \frac{precision \times recall}{precision + recall}$$

Where $precision = \frac{TP}{TP+FP}$, $recall = \frac{TP}{TP+FN}$.

To explore whether graph structures aid in the detection of cancer metastasis, we compared Graph Convolutional Networks (GCNs) and graph transformers with structure-agnostic models, such as Multi-Layer Perceptrons (MLPs) and transformers. All four models use the same architecture shown in Figure 1. When GCNs ignore the normalized Laplacian, they degrade into MLP models, resulting in GCNs and MLPs having the same number of parameters. Compared to transformers, graph transformers calculate attention scores between nodes and their neighbors instead of all other nodes, leading to the same number of trainable parameters for both models.

Table 1 shows the statistics of each model's parameters. The experimental results are shown in Table 2. GCNs perform the best, achieving approximately 90% accuracy. MLPs achieve only 73.12% accuracy, as they consider only node features and are thus limited. Similarly, transformers fall short, with an accuracy of about 72.11%, since vanilla transformers might aggregate redundant information from distant nodes. Graph transformers address this by calculating attention scores with neighboring nodes only, achieving better accuracy at about 86%. Overall, incorporating proper graph structures can significantly improve classification accuracy.

Table 2. parameters in embedding layers.

Models	Main layers	Parameters	Summary of layer wise Parameters	Model total Parameters
GCN_Net/ MLP	GCN layer 1/ Full connected layer 1	Weight matrix: $W^{(1)} \in \mathbb{R}^{d1\times d2}$, $d1 = 3$, $d2 = 64$	$d1 \times d2 = 192$	4416
		Bias vector: $b^{(1)} \in \mathbb{R}^{b1\times 1}$, $b1 = 64$	$b1 = 64$	
	GCN layer 2/ Full connected layer 2	Weight matrix: $W^{(2)} \in \mathbb{R}^{d3\times d4}$, $d3 = 64$, $d4 = 64$	$d3 \times d4 = 4096$	
		Bias vector: $b^{(1)} \in \mathbb{R}^{b2\times 1}$, $b2 = 64$	$b2 = 64$	
Transformer/ Graph Transformer	Linear transformer layer 1 $(Q^{(1)}, K^{(1)}, V^{(1)})$	Weight matrix: $(Q^{(1)}, K^{(1)}, V^{(1)}) \in \mathbb{R}^{d1\times d2}$, $d1 = 3$, $d2 = 64$	$d1 \times d2 \times 3 = 576$	13376
		Bias vector: $(Q_b^{(1)}, K_b^{(1)}, V_b^{(1)}) \in \mathbb{R}^{b1\times 1}$, $b1 = 64$	$b1 \times 3 = 256$	
	Feature aggregate layer 1 $(O^{(1)})$	Weight matrix: $O^{(1)} \in \mathbb{R}^{d3\times d4}$, $d3 = 64$, $d4 = 64$	$d3 \times d4 = 4096$	
	Linear transformer layer 2 $(Q^{(2)}, K^{(2)}, V^{(2)})$	Weight matrix: $(Q^{(2)}, K^{(2)}, V^{(2)}) \in \mathbb{R}^{d5\times d6}$, $d5 = 64$, $d6 = 64$	$d5 \times d6 = 4096$	
		Bias vector: $(Q_b^{(2)}, K_b^{(2)}, V_b^{(2)}) \in \mathbb{R}^{b2\times 1}$, $b2 = 64$	$b2 \times 3 = 256$	
	Feature aggregate layer 2 $(O^{(2)})$	Weight matrix: $O^{(2)} \in \mathbb{R}^{d7\times d8}$, $d7 = 64$, $d8 = 64$	$d7 \times d8 = 4096$	

Multi-omics integration prediction enhanced precision in diversity

To demonstrate that multi-omics data can improve performance, we conducted ablation experiments using GCN. The results comparing single-omics data and multi-omics data are shown in Fig. 3a, which presents the performance scores when testing the GCN model. In the single-omics data experiments, methylation (meth) achieves the highest accuracy at approximately 88%, while mutation performs the worst, with an accuracy of 77%. These results indicate that GCN achieves superior performance with multi-omics data compared to using any single omics data.

The ROC curve reflects the relationship between sensitivity and specificity. The abscissa represents 1-specificity, also known as the false positive rate (FPR). The closer the X-axis is to zero, the higher the accuracy. The ordinate represents sensitivity, also known as the true positive rate, with a higher Y-axis indicating better accuracy. The Area Under the Curve (AUC) is used to measure the accuracy. A higher AUC value indicates a larger area under the curve, signifying better prediction accuracy. The closer the curve is to the top-left corner (with a smaller X and a larger Y), the better the prediction accuracy. Figure 4 illustrates the ROC curve and AUC for both single-omics and multi-omics data. Among the single-omics data, mutation achieves the lowest AUC at 0.86. mRNA ranks second with an AUC of 0.92, and methylation performs best with an AUC of 0.94. Impressively, multi-omics data improves performance, achieving an AUC of 0.95.

.

Interpretation method combined with MetaGXplore provides insight into metastasis pivotal genes

Utilizing the graph mask and feature mask methodologies from GNNExplainer, genes underwent ranking based on their weights, indicative of their significance within the predictive framework. Subsequently, we identified the top 500 genes for both metastatic and non-metastatic patient prognostication, facilitating further scrutiny. Functional pathway annotation of these gene sets unveiled their involvement across diverse biological processes, encompassing RNA splicing, actin filament organization, anatomical structure homeostasis, cell killing, and regulation of RNA splicing (Fig. 5A). These processes frequently intersect with cancer metastasis mechanisms, including cell migration, invasion, and adaptation to new environments. Additionally, we presented a network visualization delineating relevant Gene Ontology (GO) terms, with larger nodes denoting a greater number of associated genes (Fig. 5B). Noteworthy pathways highlighted include T cell-mediated cytotoxicity, antigen processing, presentation via MHC class 1b, as well as various metabolic processes like sphingomyelin, sphingoglycolipid, and ceramide metabolism. This underscores the enrichment of the analyzed gene sets in biological processes and pathways pertinent to metastasis, such as cell migration, immune evasion, and metabolic reprogramming. Notably, several genes exhibited significant enrichment in RNA splicing, with a notable representation in this pathway. Among these, spliceosome components SF3B3, PRPF4B, SRRM1, and SRRM2 form a dynamic ribonucleoprotein complex assembled from small nuclear RNA (snRNA) and diverse proteins within the eukaryotic cell nucleus. Somatic mutations in pre-mRNA splicing factors represent frequent acquired mutations and early genetic events in myelodysplastic syndromes (MDS) and related myeloid tumors, alongside some solid tumors [25-27].

Conversely, genes bearing high weights associated with non-metastatic patients, as discerned through the interpretability analysis of MetaGXplore, revealed significant enrichment in novel pathways. Compared to counterparts at high metastatic risk, gene sets enriched in non-metastatic patients manifested fresh biological pathways, including regulation of macroautophagy, cellular component assembly, intermediate filament cytoskeleton organization, and positive regulation of cell killing. These pathways may serve to impede or deter metastatic progression by mechanisms such as bolstering tumor cell self-clearance, sustaining cellular structural integrity, and augmenting anti-tumor immune responses. This discovery furnishes a theoretical foundation for elucidating the molecular orchestration of metastasis and advancing novel anti-metastatic targeted therapies.

Conclusion

In this research endeavor, we have devised a pioneering deep learning model aimed at forecasting the likelihood of metastasis occurrence in patients afflicted with various cancers. Employing an interpretable

framework, we have discerned a pivotal set of genes whose role in prediction is pronounced and possibly intertwined with tumor metastasis. Our findings offer a valuable resource for healthcare practitioners, furnishing them with a predictive tool for gauging the metastatic risk on a per-patient basis. Furthermore, the elucidation of this gene set lends insights into the underlying biological mechanisms governing metastasis, enriching our understanding of this intricate process.

Data available statement

Publicly available datasets were analyzed in this study. This data can be found here: The 754 cancer samples were obtained from the The Cancer Genome Atlas (TCGA; https://www.cancer.gov/). Access data and model for this article are listed in https://github.com/TJiangBio/MetaGXplore.

Funding

References

[1] D. R. Robinson *et al.*, "Integrative clinical genomics of metastatic cancer," *Nature,* vol. 548, no. 7667, pp. 297-303, Aug 17 2017, doi: 10.1038/nature23306.

[2] X. Guan, "Cancer metastases: challenges and opportunities," *Acta Pharm Sin B,* vol. 5, no. 5, pp. 402-18, Sep 2015, doi: 10.1016/j.apsb.2015.07.005.

[3] S. Ramaswamy, K. N. Ross, E. S. Lander, and T. R. Golub, "A molecular signature of metastasis in primary solid tumors," *Nat Genet,* vol. 33, no. 1, pp. 49-54, Jan 2003, doi: 10.1038/ng1060.

[4] C. Li *et al.*, "Integrated Omics of Metastatic Colorectal Cancer," *Cancer Cell,* vol. 38, no. 5, pp. 734-747 e9, Nov 9 2020, doi: 10.1016/j.ccell.2020.08.002.

[5] F. Bray, J. Ferlay, I. Soerjomataram, R. L. Siegel, L. A. Torre, and A. Jemal, "Global cancer statistics 2018: GLOBOCAN estimates of incidence and mortality worldwide for 36 cancers in 185 countries," *CA Cancer J Clin,* vol. 68, no. 6, pp. 394-424, Nov 2018, doi: 10.3322/caac.21492.

[6] E. R. Malone, M. Oliva, P. J. B. Sabatini, T. L. Stockley, and L. L. Siu, "Molecular profiling for precision cancer therapies," *Genome Med,* vol. 12, no. 1, p. 8, Jan 14 2020, doi: 10.1186/s13073-019-0703-1.

[7] B. U. Sevin and H. Graeff, "Principles of staging laparotomy in ovarian cancer," *Chirurg,* vol. 65, no. 1, pp. 2-9, Jan 1994. [Online]. Available: https://www.ncbi.nlm.nih.gov/pubmed/8149795. Prinzip der Staging-Laparotomie beim Ovarialcarcinom.

[8] J. Fares, M. Y. Fares, H. H. Khachfe, H. A. Salhab, and Y. Fares, "Molecular principles of metastasis: a hallmark of cancer revisited," *Signal Transduct Target Ther,* vol. 5, no. 1, p. 28, Mar 12 2020, doi: 10.1038/s41392-020-0134-x.

[9] D. Hanahan, "Hallmarks of Cancer: New Dimensions," *Cancer Discov,* vol. 12, no. 1, pp. 31-46, Jan 2022, doi: 10.1158/2159-8290.CD-21-1059.

[10] D. Hanahan and R. A. Weinberg, "Hallmarks of cancer: the next generation," *Cell,* vol. 144, no. 5, pp. 646-74, Mar 4 2011, doi: 10.1016/j.cell.2011.02.013.

[11] Y. Hasin, M. Seldin, and A. Lusis, "Multi-omics approaches to disease," *Genome Biol,* vol. 18, no. 1, p. 83, May 5 2017, doi: 10.1186/s13059-017-1215-1.

[12] N. Rahimzadeh, S. S. Srinivasan, J. Zhang, and V. Swarup, "Gene networks and systems biology in Alzheimer's disease: Insights from multi-omics approaches," *Alzheimers Dement,* vol. 20, no. 5, pp. 3587-3605, May 2024, doi: 10.1002/alz.13790.

[13] M. Mounir *et al.*, "New functionalities in the TCGAbiolinks package for the study and integration of cancer data from GDC and GTEx," *PLoS Comput Biol,* vol. 15, no. 3, p. e1006701, Mar 2019, doi:

10.1371/journal.pcbi.1006701.
[14] E. Bernard *et al.*, "Molecular International Prognostic Scoring System for Myelodysplastic Syndromes," *NEJM Evid,* vol. 1, no. 7, p. EVIDoa2200008, Jul 2022, doi: 10.1056/EVIDoa2200008.
[15] K. Chaudhary, O. B. Poirion, L. Lu, and L. X. Garmire, "Deep Learning-Based Multi-Omics Integration Robustly Predicts Survival in Liver Cancer," *Clin Cancer Res,* vol. 24, no. 6, pp. 1248-1259, Mar 15 2018, doi: 10.1158/1078-0432.CCR-17-0853.
[16] H. Chereda, A. Bleckmann, F. Kramer, A. Leha, and T. Beissbarth, "Utilizing Molecular Network Information via Graph Convolutional Neural Networks to Predict Metastatic Event in Breast Cancer," *Stud Health Technol Inform,* vol. 267, pp. 181-186, Sep 3 2019, doi: 10.3233/SHTI190824.
[17] Y. Yang, V. Tresp, M. Wunderle, and P. A. Fasching, "Explaining Therapy Predictions with Layer-Wise Relevance Propagation in Neural Networks," presented at the 2018 IEEE International Conference on Healthcare Informatics (ICHI), 2018.
[18] P. a. C. o. t. E. Union., "General data protection regulation," 2016. [Online]. Available: https://gdpr-info.eu/.
[19] A. Vaswani *et al.*, "Attention Is All You Need," *Advances in neural information processing systems,* vol. 30, 2017.
[20] Y. Shi, Z. Huang, S. Feng, H. Zhong, W. Wang, and Y. Sun, "Masked Label Prediction: Unified Message Passing Model for Semi-Supervised Classification," *arXiv preprint arXiv,* vol. 2009.03509, 2020.
[21] M. Welling and T. N. Kipf, "SEMI-SUPERVISED CLASSIFICATION WITH GRAPH CONVOLUTIONAL NETWORKS," *In J. International Conference on Learning Representations,* 2016.
[22] H. Zhao, J. Liu, Z. Shen, and J. Yan, "SCC-MPGCN: self-attention coherence clustering based on multi-pooling graph convolutional network for EEG emotion recognition," *J Neural Eng,* vol. 19, no. 2, Apr 21 2022, doi: 10.1088/1741-2552/ac6294.
[23] J. Lee, I. Lee, and J. Kang, "Self-attention graph pooling," *In International conference on machine learning,* 2019.
[24] R. Ying, D. Bourgeois, J. You, M. Zitnik, and J. Leskovec, "GNNExplainer: Generating Explanations for Graph Neural Networks," *Adv Neural Inf Process Syst,* vol. 32, pp. 9240-9251, Dec 2019. [Online]. Available: https://www.ncbi.nlm.nih.gov/pubmed/32265580.
[25] J. L. Jenkins and C. L. Kielkopf, "Splicing Factor Mutations in Myelodysplasias: Insights from Spliceosome Structures," *Trends Genet,* vol. 33, no. 5, pp. 336-348, May 2017, doi: 10.1016/j.tig.2017.03.001.
[26] S. Chen, S. Benbarche, and O. Abdel-Wahab, "Splicing factor mutations in hematologic malignancies," *Blood,* vol. 138, no. 8, pp. 599-612, Aug 26 2021, doi: 10.1182/blood.2019004260.
[27] Y. Zhao, W. Cai, Y. Hua, X. Yang, and J. Zhou, "The Biological and Clinical Consequences of RNA Splicing Factor U2AF1 Mutation in Myeloid Malignancies," *Cancers (Basel),* vol. 14, no. 18, Sep 10 2022, doi: 10.3390/cancers14184406.

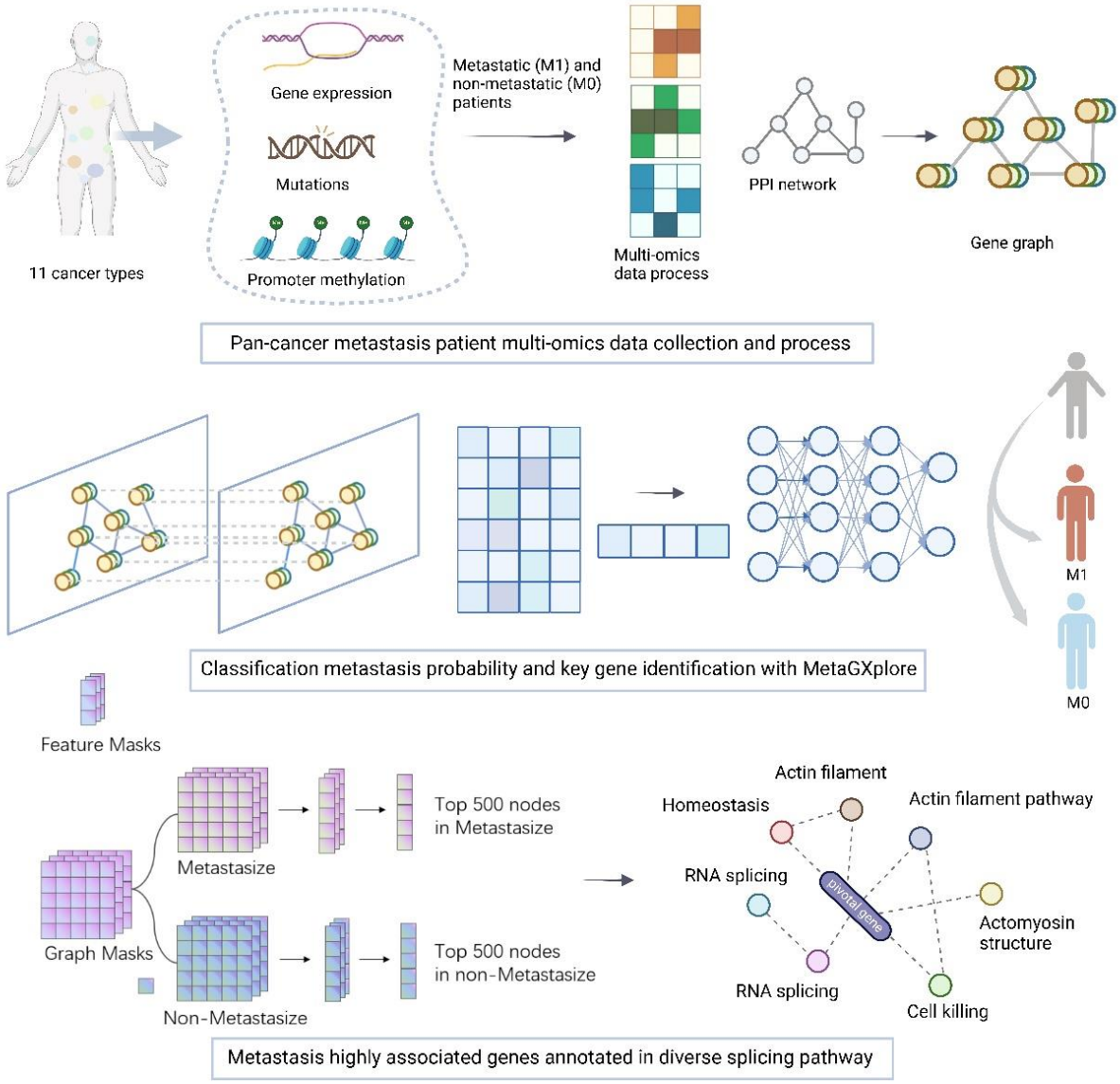

Figure 1. The schematic map of MetaGXplore and explainable method for metastasis-related gene identification.

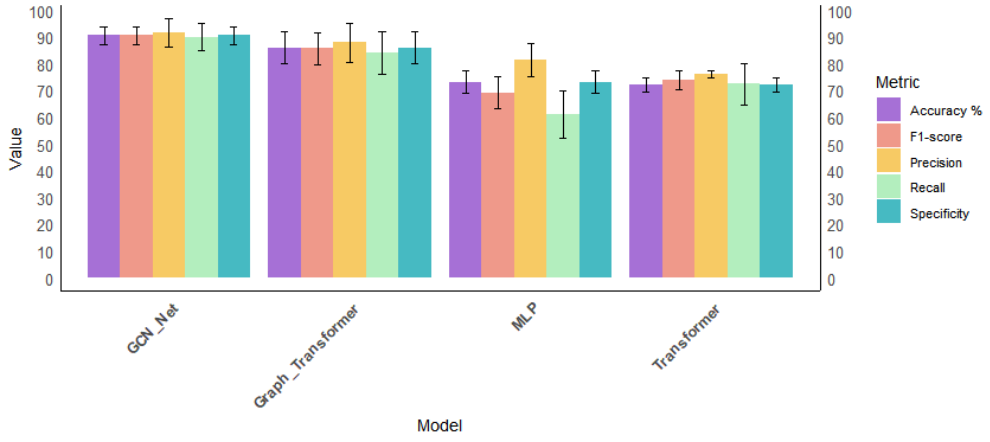

Figure 3. Performance of four embedding models.

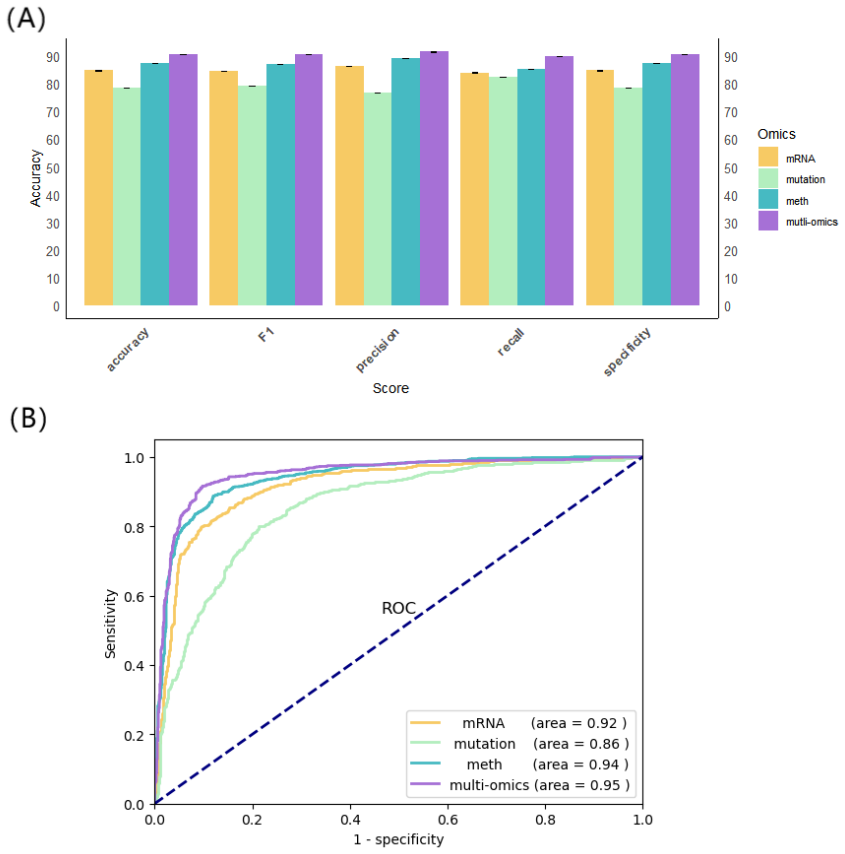

Figure 4. Accuracy and ROC comparison between multi-omics and single omic data

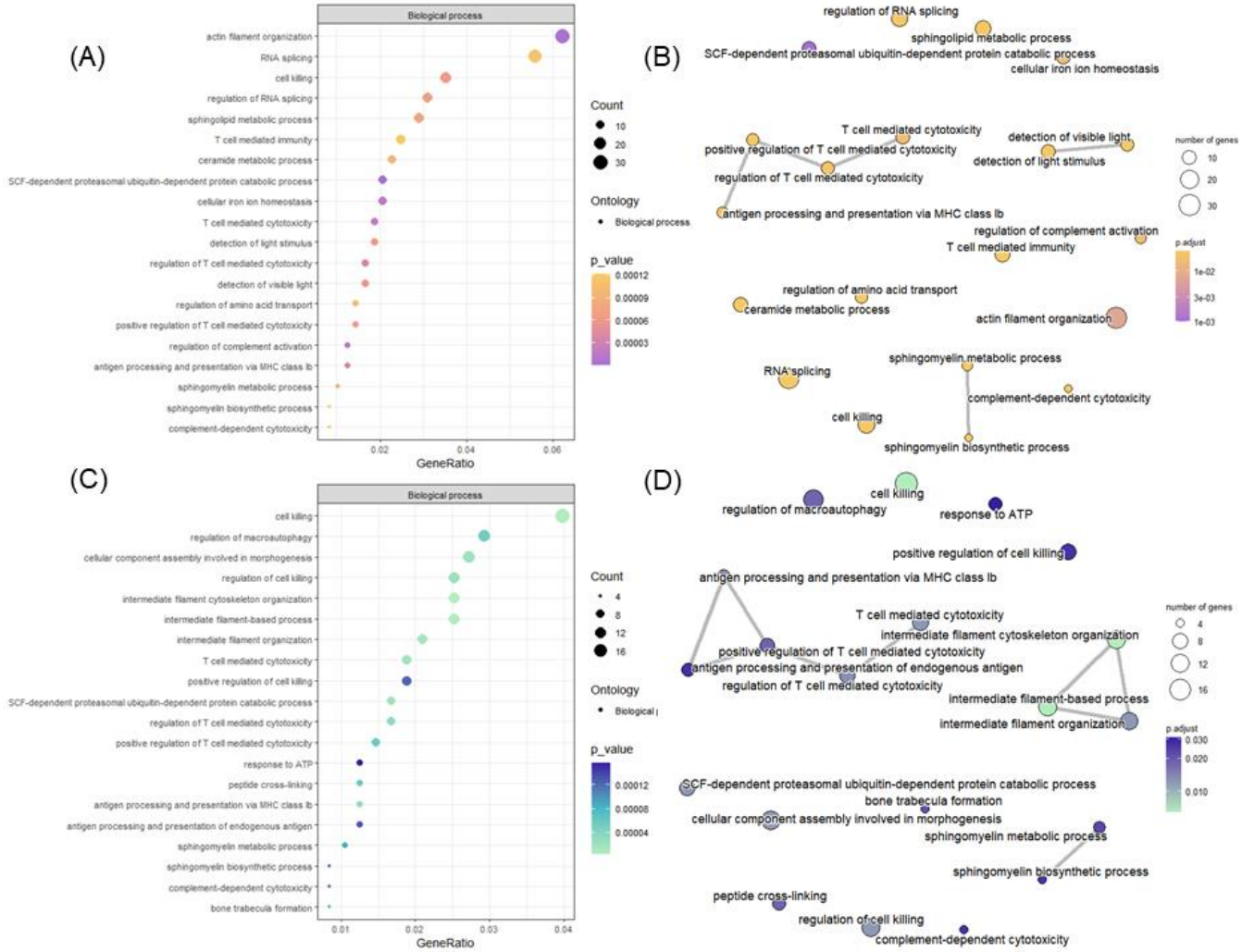

Figure 5. Enrichment analysis of the pivotal genes. (a) The top 500 genes associated with metastasis interpreted from MetaGXplore were enriched for biological functional pathways, showing the top twenty significantly enriched pathways. (b) Relationship between pathways of metastasis prediction-related genes. (c-d) The top 500 genes related to non-metastasis prediction were enriched in biological pathways and the relationships between pathways.